Update of Chilean jack mackerel CPUE abundance index estimated by spatiotemporal SPDE-based models using sdmTMB.

By Ignacio S. Payá C.

May 2026.

Stock Assessment Department.

Chilean Fisheries Development Institute.

Abstract

The CPUE index of the Central-South Chile purse seiner fleet is one of the most important indices of the Chilean Jack Mackerel stock assessment model. The CPUE is calculated as the catch divided by the days off port multiply by the vessel holding capacity (hc). Since 2023 alternative indices based on catch by fishing set have been fitted. These alternative indices have been estimated using spatiotemporal SPDE-Based models with sdmTMB package. The aim of this report is to update these indices with electronic logbooks until first semester 2025. Two types of models were fitted, a spatiotemporal model with a spline of the vessel holding capacity (s(hc)), where the annually variability was modelled by spatiotemporal random fields with a first-order autoregressive process, and a spatiotemporal GLMM with year and month as fixed effects and s(hc), where the annually variability was estimated using the year fixed effect. A new regular mesh with a reference hc was used to predict the abundance indices. These regular mesh indices were similar to the index based on the year fixed effect of the spatiotemporal GLMM. Therefore, the index based on the year effect is recommended. Because of sample size limitations this index should be used starting from year 2000.

Background.

The CPUE index of the Central-South Chile purse seiner fleet is one of the most important indices of the Chilean Jack Mackerel stock assessment model. The CPUE is calculated as the catch divided by the days off port multiply by the vessel holding capacity (Canales et al. 2008) and annually updated (Payá 2025a). An alternative index based on catch by fishing set was estimated by GLM using a statistical model that included a distribution of compound probability that describes the joint probability of success and catch per fishing set (Caballero et al., 2020 and Payá, 2023b). However, this model explained 10.2% of total deviance and had small sample sizes in some years, therefore, further analyses were identified. Payá (2023c) estimated CPUE indices using spatiotemporal SPDE-Based GLMMs with template model builder (sdmTMB). Two models were fitted to the data, a spatiotemporal model, where the annually variability is modelled by spatiotemporal random fields with autoregressive time correlation, and a spatiotemporal GLMM, where the annually variability is

estimated using the year fixed effect. The estimated abundance indices were not significantly different between the two models (Figure 1).

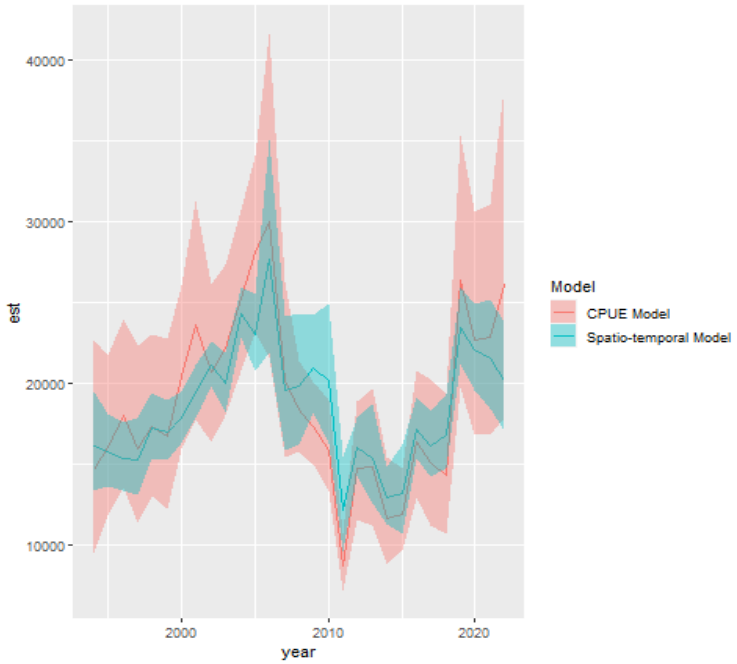


Figure 1. Abundance index estimated by the CPUE spatiotemporal GLM model (CPUE model) and by spatiotemporal model using sdmTMB.

In relation to the CPUE index estimated by GLM using catch per fishing set (Caballero et al., 2020 and Payá, 2023b), the indices had similar trends. In relation to the CPUE abundance index used in the stock assessment model (2023a), the indices had a similar trend for the 2006-2022 period, but not for the 1994-2005 period (Figure 2). For the 2006-2022 period all indices showed a "V" type trend with the minimal figure at year 2011, but the rate of decrease before this year and the rate of increase after this year was greater in the abundance index based on fishing trips.

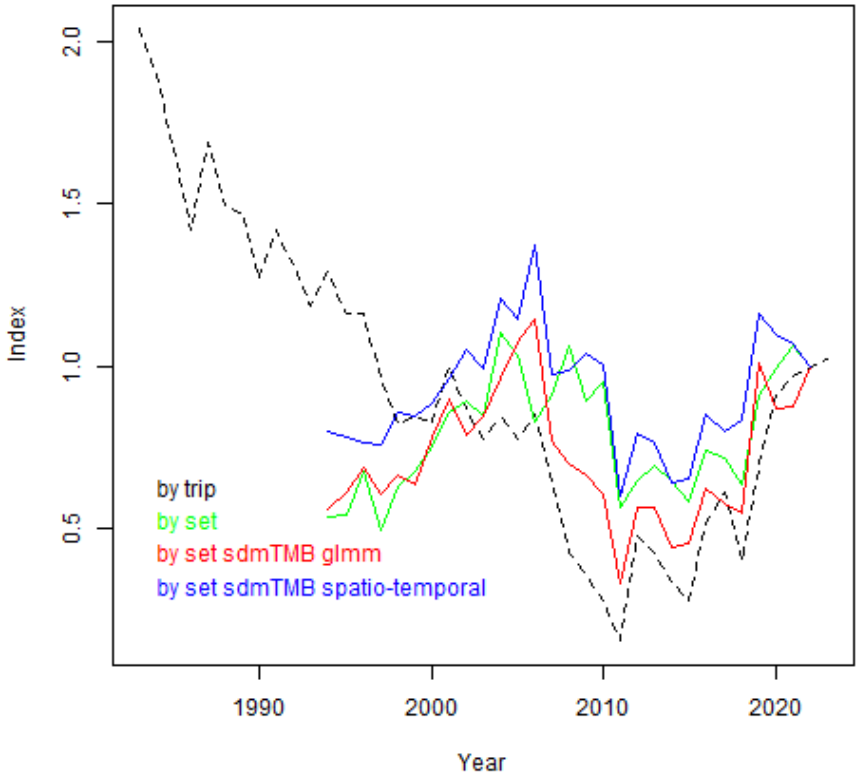


Figure 2. Abundance indices estimated by different models. CPUE index used in the stock assessment model updated up to June 2023 (trip), CPUE index based on GLM of catch per fishing set (set), CPUE estimated by the spatiotemporal model (by set sdmTMB spatio-temporal) and CPUE index estimated by the spatiotemporal GLM (by set sdmTMB glm). Indices were divided by their values in 2022 year.

Aim

To estimate a Chilean jack mackerel abundance index using spatiotemporal SPDE-based GLM with template model builder (sdmTMB).

Data

The database covered from 1994 to the first semester of 2025, with two time periods with different data sources. The first period (1994-2022) was composed by the daily logbooks of fishing sets associated to the industrial purse seine fleet that operated in the Chilean central-south macro zone (Caballero et al., 2020, Payá, 2023c). The records were from the IFOP scientific observers on board fishing vessels for June/1994–December/2022 period that were supplemented with INPESCA records of the fishing industry logbooks for June/1994–April/2022 period. The second period (2023-1st semester 2025) was composed by electronic logbooks provided by Chilean National Marine Fisheries and Aquaculture Service (www.sernapesca.cl), and they included the whole fishing fleet.

The fishing set location in latitude and longitude units were transformed to UTM using EPSG: 32718 – WGS 84 / UTM zone 18S (https://maps.omniscale.com/en/openstreetmap/epsg-32718) (Figure 3)

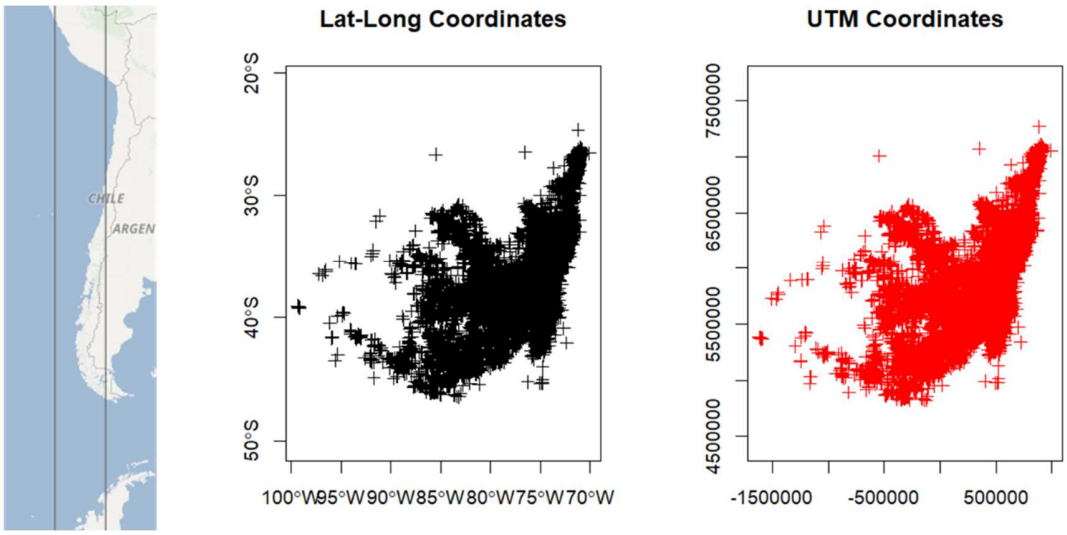


Figure 3. The left map shows the box area of the coordinate reference system according to the EPSG: 32718 – WGS 84 / UTM zone 18S. The fishing set locations in latitude-longitude units (centre plot) and UTM coordinates (right plot) for the 1994-2025 period.

Methods

To discretize space, a mesh was constructed to generate a set of neighboring points at which spatial autocorrelation can be evaluated. A triangular mesh was used because it is more flexible and can adapt to irregular domains (Figure 4). The sdmTMB code was

```
bnd_5 <- INLA::inla.nonconvex.hull(cbind(cjm$X, cjm$Y), convex = -3.8/1000)

mesh_5 <- make_mesh(cjm, c("X", "Y"),  fmesher_func = fmesher::fm_mesh_2d_inla,
            boundary = bnd_5,   cutoff = 30,  max.edge = c(600,600), offset = c(5,3))
```

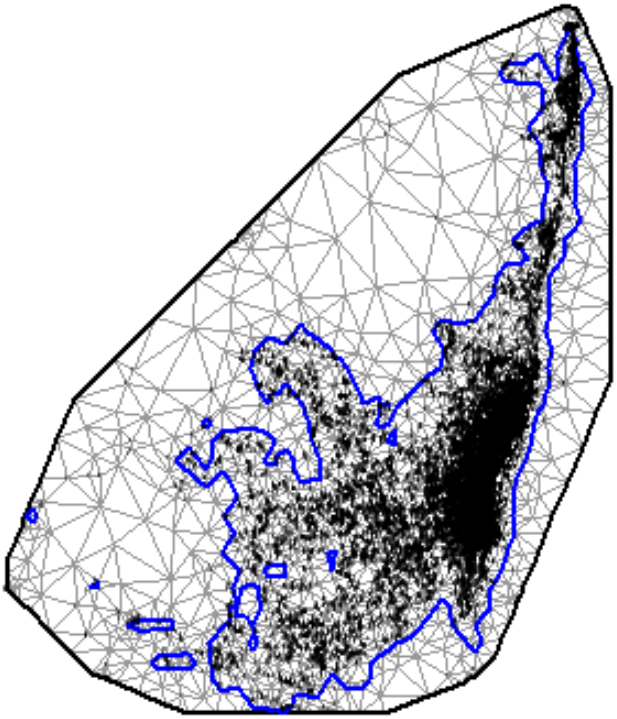


Figure 4. Mesh with the original data.

The SPDE (Stochastic Partial Differential Equation) approach was used to represent the spatial autocorrelation structure of the database at the mesh vertices. In this framework, the SPDE provides a computationally efficient representation of a Matérn Gaussian random field. The Matérn covariance function can be written as:

$$Cov(S(x_i), S(x_j)) = \frac{\sigma^2}{2^{\upsilon-1}\Gamma(\nu)} (\kappa \|x_i - x_j\|)^{\nu} \kappa_{\nu}(\kappa \|x_i - x_j\|)$$

where K_ν(·) is the modified Bessel function of the second kind of order ν>0; ν is the smoothness parameter; σ^2 is the marginal variance; and κ>0 is a spatial scale parameter related to the practical range. The practical range is commonly defined as ρ = √(8ν)/κ, i.e., the distance at which the spatial correlation is approximately 0.1.

Two models were fitted; both included anisotropy.

Spatiotemporal model

CPUE (density) was modelled as a smooth function of vessel hold capacity (hc), with spatiotemporal variability specified as a first-order autoregressive process (AR1). A Tweedie error distribution with a log link was used (Dunn, 2017). The sdmTMB specification was:

```
fit_spatiotemporal <- sdmTMB( density ~ s(hc, k = 5), data = cjm, mesh = mesh, time = "year", family
                      = tweedie(link = "log"), spatial = "off", spatiotemporal = "ar1", anisotropy =
                      TRUE, control = sdmTMBcontrol(newton_loops = 1))
```

and can be written on the linear predictor scale as:

$$g(\mu_{s,t}) = S(hc, k = 5) + \delta_{s,t},$$
$$\delta_{t=1} \sim MVNormal(0, \Sigma_\epsilon),$$
$$\delta_{t>1} \sim \rho\delta_{t-1} + \sqrt{1-\rho^2}\epsilon_t, \ \epsilon \sim MVNormal(0, \Sigma_\epsilon)$$

where g(·) is the link function; μ is the mean density (CPUE); s denotes spatial location (x and y coordinates); t is time; S(·) is a smoothing spline with basis dimension k; δ are spatiotemporal deviations; Σ_ϵ is the covariance matrix of the spatiotemporal random fields; and ρ is the correlation between consecutive spatiotemporal fields. This scaling yields a steady-state (marginal) variance. The parameter ρ allows mean-reverting spatiotemporal fields and is constrained to $-1 < \rho < 1$.

To estimate an area-weighted standardized population index by year, the original dataset mesh was replicated across years:

```
grid_yrs <- replicate_df(cjm, "year", unique(cjm$year))
```

Predictions were generated from the fitted model (fit_spatiotemporal) using the original data mesh (grid_yrs):

```
p_st <- predict(fit_spatiotemporal, newdata = grid_yrs, return_tmb_object = TRUE)
```

Then, using the predictions (p_st), the index was extracted as:

```
index0 <- get_index(p_st, area = rep(4, nrow(grid_yrs)))
```

To evaluate the effect of the prediction locations used to build the index, a **new mesh** with regular positions was generated. Using the boundary object (bnd_5), minimum and maximum coordinates were taken and regular positions were created.

```
predictor_dat <- expand.grid( X = seq(xMIM, xMAX, length.out = 30), Y = seq(yMIM, yMAX,
                 length.out = 150))
```

These were then used to generate a new prediction mesh:

```
mesh_5_pred2 <- make_mesh(predictor_dat, c("X", "Y"), cutoff = 20, boundary = bnd_5)
```

From this mesh, the locations were extracted (Figure 8):

```
predictor_dat2<-as.data.frame(cbind(mesh_5_pred2$mesh$loc[,1],mesh_5_pred2$mesh$loc[,2]))
```

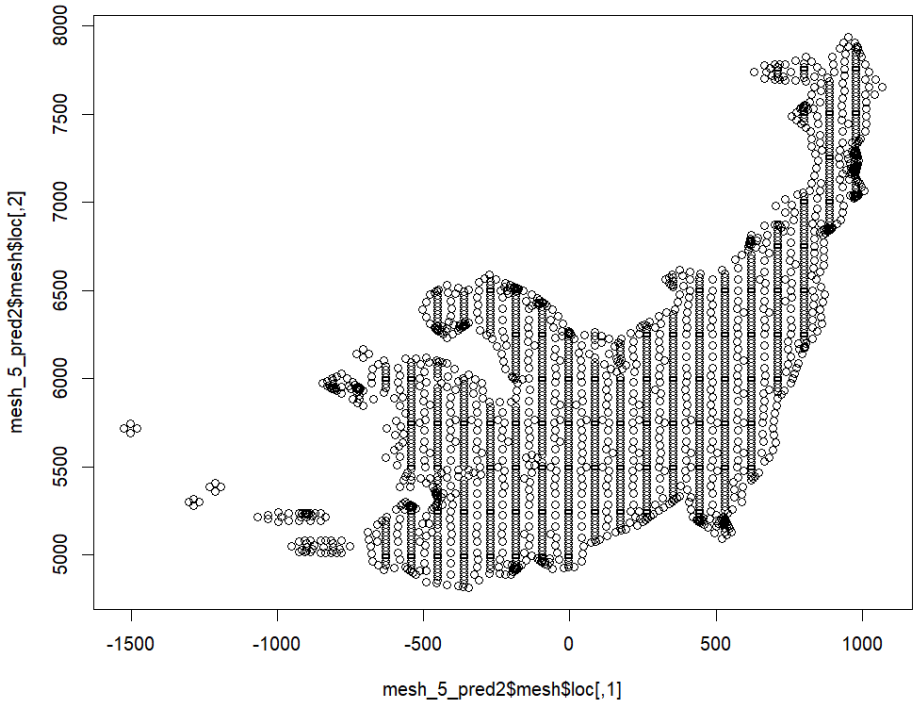


Figure 5. Regular locations used to generate new data for prediction.

Finally, the new prediction dataset was generated by replicating locations across years and months and setting a reference hold capacity of 1458 m^3.

```
grid_yrs_pred <- replicate_df(predictor_dat2, "year",sort(unique(cjm$year)))

grid_yrs_pred_month <- replicate_df(grid_yrs_pred, "month", 1:12)

grid_yrs_pred_month_CB <- replicate_df(grid_yrs_pred_month, "CB", 1458)
```

Using the new data, predictions were generated for the regular grid:

```
p_st_Cuadrada <- predict(fit_spatiotemporal, newdata = grid_yrs_pred_month_CB,
                         return_tmb_object = TRUE)
```

and the index was estimated as:

```
index0Cuadrada <- get_index(p_st_Cuadrada, area = 4, bias_correct = TRUE)
```

Spatiotemporal GLMM

CPUE (density) was modelled as function of year and month fixed effects plus a smooth function of vessel hold capacity (hc), with spatiotemporal variability specified as a first-order autoregressive process (AR1). A Tweedie error distribution with a log link was used (Dunn, 2017). The sdmTMB specification was:

```
m <- sdmTMB(data = cjm, formula = density ~ 0 + as.factor(year) + as.factor(month) + s(hc, k = 5),
    time = "year", mesh = mesh, family = tweedie(link = "log", anisotropy = TRUE, control =
    sdmTMBcontrol(newton_loops = 1))
```

and can be written on the linear predictor scale as:

$$g(\mu_{s,t}) = \mathrm{X}_{s,t}^{\mathrm{main}}\beta + S(hc, k = 5) + \epsilon_{s,t}$$

Where $\mathrm{X}_{s,t}^{\mathrm{main}}$ is the design matrix for the main effects (year and month), β is the fixed-effect coefficient vector, and $\epsilon_{s,t}$ are iid spatiotemporal random fields.

$$\epsilon_{s,t} \sim \mathrm{MVNormal}(0, \Sigma\epsilon).$$

For a regional-index exercise, south (<6000 UTM Northing) vs north (≥6000 UTM Northing) and west (<500 UTM Easting) vs east (≥500 UTM Easting) areas were defined.

Results

Spatiotemporal model

A summary of the spatiotemporal model results is shown in Table 1.

Table 1. Summary of the spatiotemporal model results.

```
Spatiotemporal model fit by ML ['sdmTMB']
Formula: density ~ s(CB, k = 5)
Mesh: mesh (anisotropic covariance)
Time column: year
Data: cjm
Family: tweedie(link = 'log')

Conditional model:
            coef.est coef.se
(Intercept)    -2.01    0.03
sCB             0.08    0.03

Smooth terms:
          Std. Dev.
sd__s(CB)      0.68
```

```
Dispersion parameter: 0.32
Tweedie p: 1.54
Spatiotemporal AR1 correlation (rho): 0.32
Matérn anisotropic range (spatiotemporal): 127.9 to 218.0 at 65 deg.
Spatiotemporal marginal AR1 SD: 0.50
ML criterion at convergence: -22386.265
```

The anisotropic was significant and the smooth term for hold capacity (hc) increased with catch per set, approaching an asymptote for larger vessels (Figure 6).

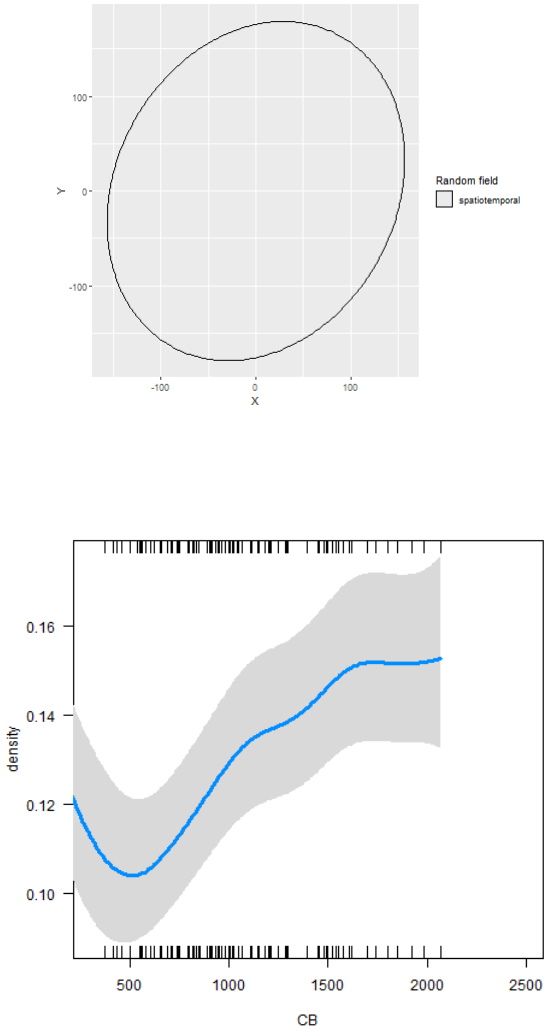


Figure 6. Anisotropy (upper panel) and the asymptotic relationship between the smooth term for hold capacity (CB = hc) and catch per set (density) (lower panel).

The centre of gravity historically shifted southward and toward coastal areas in more recent years (Figure 7).

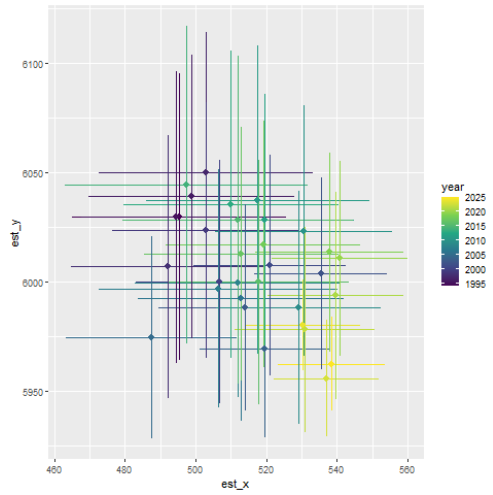


Figure 7. Centres of gravity by year estimated using the spatiotemporal model; lines indicate 95% intervals.

The abundance index showed a cyclic pattern with increases in 1994–2004, decreases in 2005–2014, increases in 2015–2019, and relative stabilization since 2020, although with higher variability in the most recent years (Figure 8).

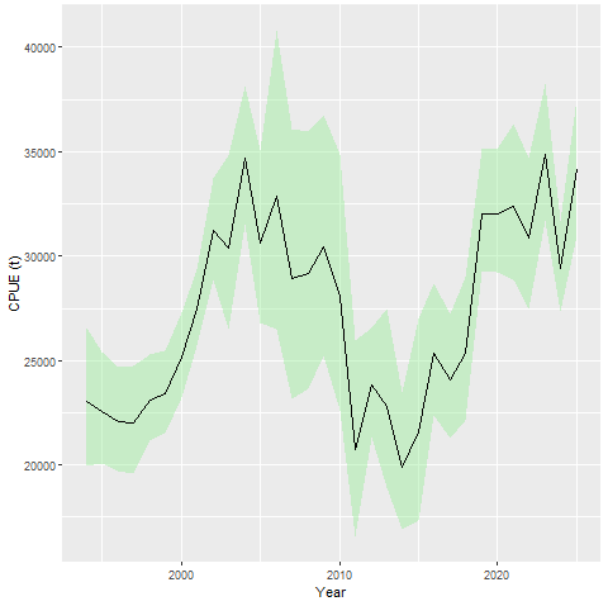


Figure 8. Abundance index estimated using the spatiotemporal model. The green band indicates 95% intervals.

Spatiotemporal GLMM

A summary of the GLMM results is presented in Table 2 and the abundance index in Table 3.

Table 2. Parameters estimated by the spatiotemporal GLMM.

	coef.est	coef.se
as.factor(year)1994	-2.10	0.20
as.factor(year)1995	-2.01	0.13
as.factor(year)1996	-1.97	0.12
as.factor(year)1997	-2.15	0.15
as.factor(year)1998	-2.04	0.12
as.factor(year)1999	-2.05	0.13
as.factor(year)2000	-1.83	0.10
as.factor(year)2001	-1.70	0.12
as.factor(year)2002	-1.82	0.10
as.factor(year)2003	-1.70	0.08
as.factor(year)2004	-1.58	0.08
as.factor(year)2005	-1.48	0.08
as.factor(year)2006	-1.46	0.14
as.factor(year)2007	-1.81	0.11
as.factor(year)2008	-1.88	0.07
as.factor(year)2009	-1.97	0.06
as.factor(year)2010	-2.07	0.08
as.factor(year)2011	-2.66	0.09
as.factor(year)2012	-2.19	0.10
as.factor(year)2013	-2.14	0.12
as.factor(year)2014	-2.41	0.12
as.factor(year)2015	-2.37	0.09
as.factor(year)2016	-2.06	0.10
as.factor(year)2017	-2.14	0.13
as.factor(year)2018	-2.21	0.13
as.factor(year)2019	-1.63	0.12
as.factor(year)2020	-1.75	0.13
as.factor(year)2021	-1.74	0.14
as.factor(year)2022	-1.72	0.17
as.factor(year)2023	-2.08	0.10
as.factor(year)2024	-1.95	0.10
as.factor(year)2025	-1.90	0.10
as.factor(month)2	-0.04	0.02
as.factor(month)3	0.02	0.02
as.factor(month)4	0.07	0.02
as.factor(month)5	0.05	0.02
as.factor(month)6	0.02	0.03
as.factor(month)7	-0.09	0.03
as.factor(month)8	-0.19	0.03
as.factor(month)9	-0.42	0.04
as.factor(month)10	-0.50	0.04
as.factor(month)11	-0.49	0.04
as.factor(month)12	-0.24	0.03
sCB	0.10	0.02

```
Smooth terms:
           Std. Dev.
sd__s(CB)      0.88

Dispersion parameter: 0.31
Tweedie p: 1.54
Matérn anisotropic range (spatial): 94.4 to 154.5
at 65 deg.
Spatial SD: 0.13
Spatiotemporal IID SD: 0.40

ML criterion at convergence: -22754.600
```

Table 3. Abundance index estimated using the spatiotemporal GLMM.

year	est	lwr	upr	cv
1994	22012	16786	28865	0.14
1995	22511	19173	26430	0.08
1996	22415	19149	26236	0.08
1997	20678	17475	24469	0.09
1998	23332	20651	26362	0.06
1999	23557	20843	26624	0.06
2000	27815	25078	30850	0.05
2001	33307	30165	36775	0.05
2002	32324	29607	35289	0.04
2003	31649	27644	36234	0.07
2004	37905	34360	41815	0.05
2005	35836	31332	40986	0.07
2006	43749	33313	57455	0.14
2007	28964	23183	36188	0.11
2008	29735	25022	35336	0.09
2009	27959	23768	32889	0.08
2010	25298	20950	30550	0.10
2011	12993	10729	15736	0.10
2012	21469	18973	24294	0.06
2013	21396	17243	26549	0.11
2014	16186	13397	19555	0.10
2015	17522	14207	21609	0.11
2016	23853	20760	27406	0.07
2017	21491	18337	25186	0.08
2018	21672	18308	25654	0.09
2019	34780	30611	39516	0.07
2020	32668	28716	37163	0.07
2021	33303	28227	39291	0.08
2022	32960	26916	40360	0.10
2023	32263	29287	35541	0.05
2024	29961	27658	32455	0.04
2025	32717	29514	36269	0.05

Residuals showed an adequate spatiotemporal distribution with no apparent spatial or temporal trend (Figures 9 and 10).

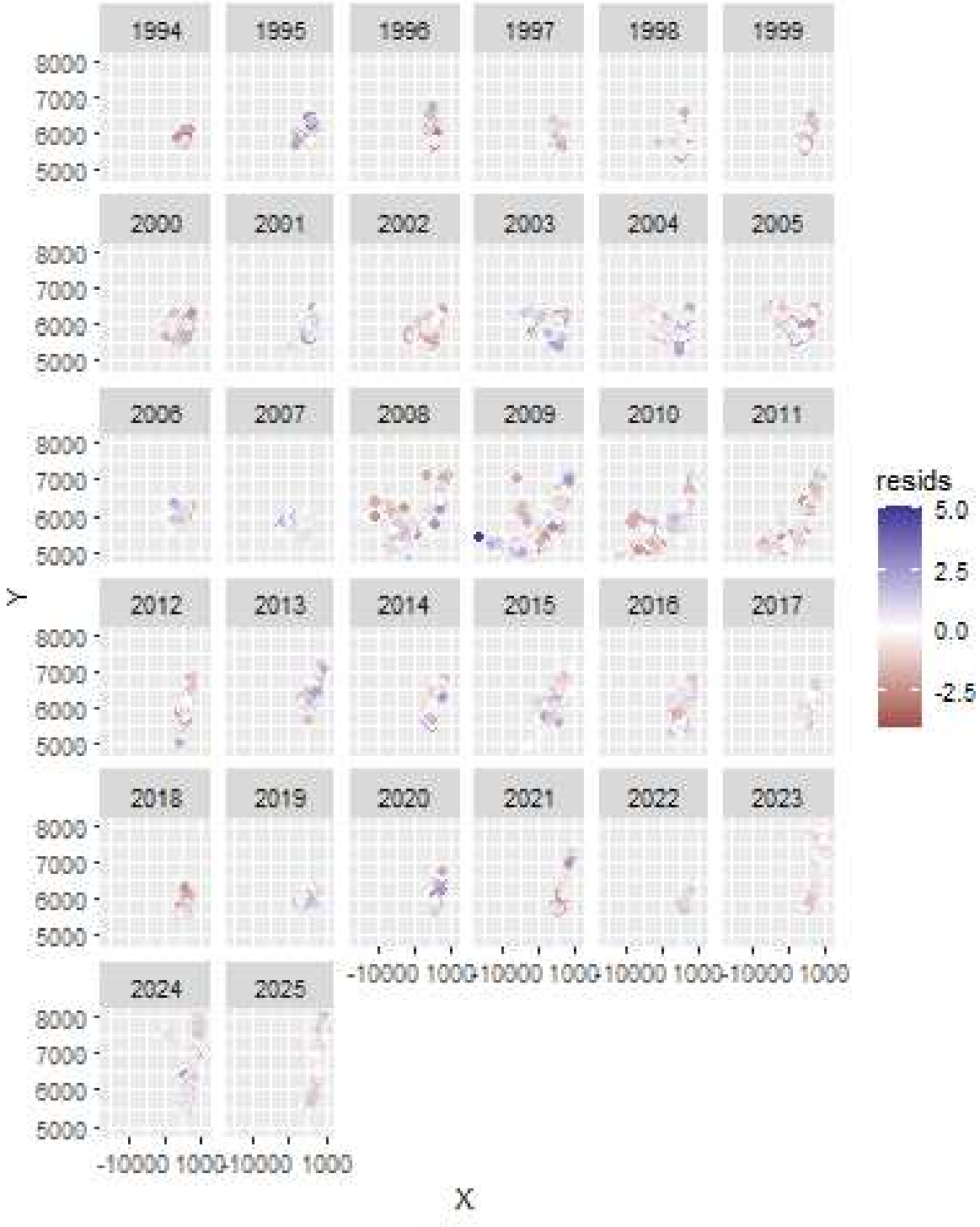


Figure 9. Residuals from the spatiotemporal GLMM by year (X = Easting, Y = Northing).

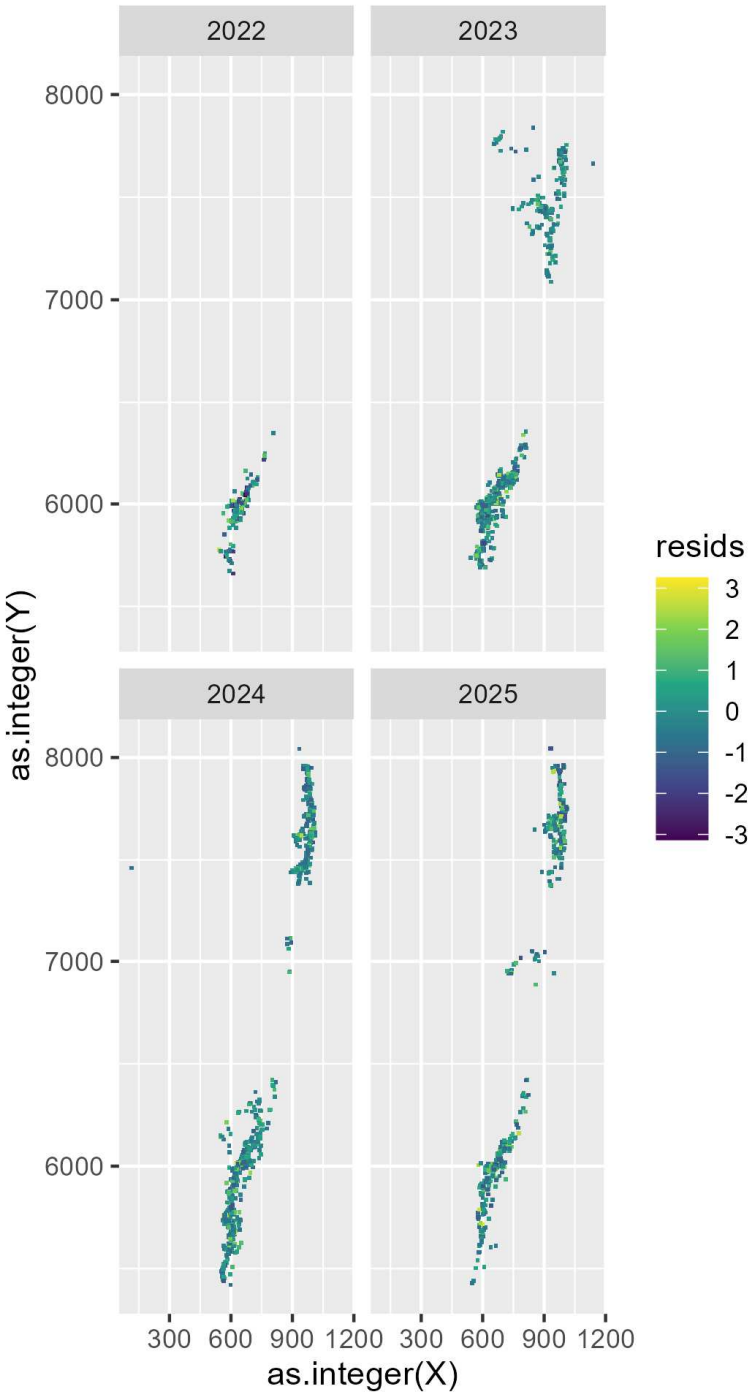


Figure 10. Example of residual diagnostics and anisotropy detail for the spatiotemporal GLMM for four years.

Indices derived from the model fixed effects showed a cyclic historical pattern with a decreasing trend in the last 4 years, and a clear seasonality with the higher abundances in the first half of the year (Figure 11).



Figure 11. Annual (top) and monthly (bottom) abundance indices estimated from the fixed effects of the spatiotemporal GLMM. The green band indicates 95% intervals.

Predictions (fixed effects plus spatiotemporal random effects) at observed set locations for the four most recent years show increasing coastal concentration of the resource (Figure 12). Predictions toward the northern extreme and offshore areas were very low.

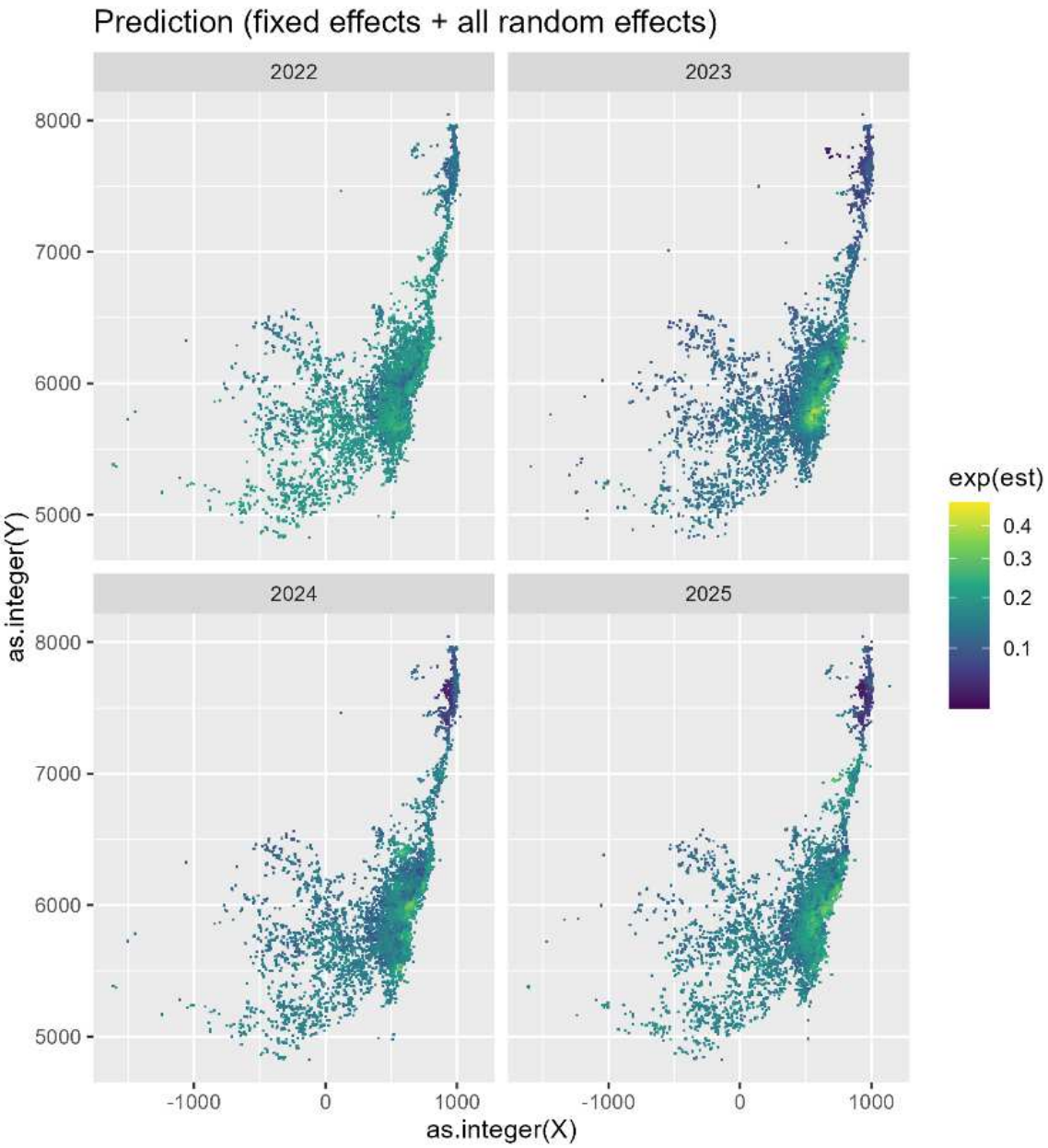


Figure 12. Example predictions from the spatiotemporal GLMM for four years.

Distribution changes and concentration areas were more evident when examining predictions based only on the spatiotemporal (random) effects (Figure 13).

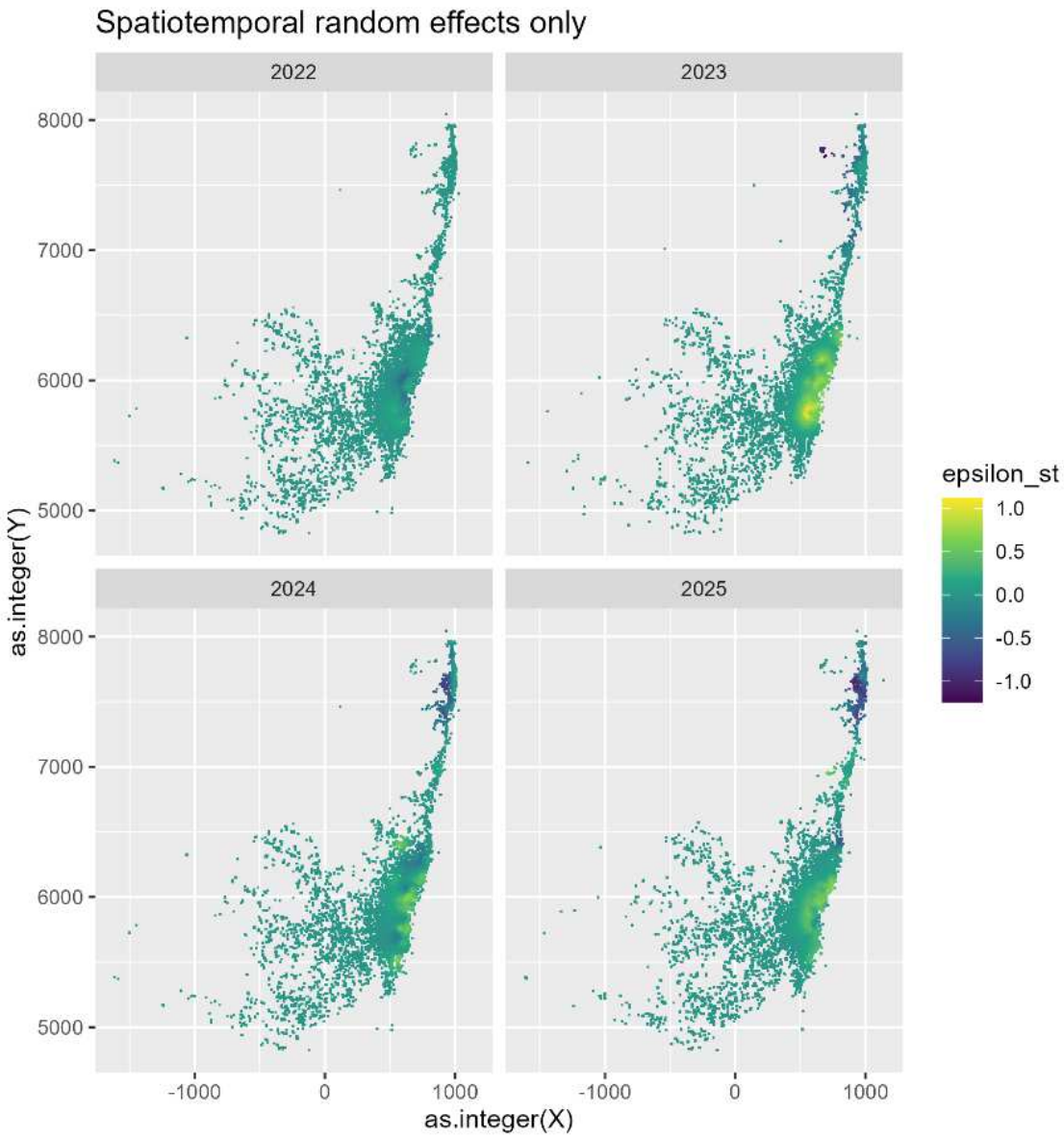


Figure 13. Example of the spatiotemporal (random) effect from the spatiotemporal GLMM for four years.

The abundance index predicted by the spatiotemporal GLMM increased during 1994–2006, decreased during 2007–2014, increased during 2015–2019, and decreased over the last five years (Figure 14). The predicted index trend was similar to the index derived from the fixed year effect, except in the most recent years where the rate of decline was smaller.

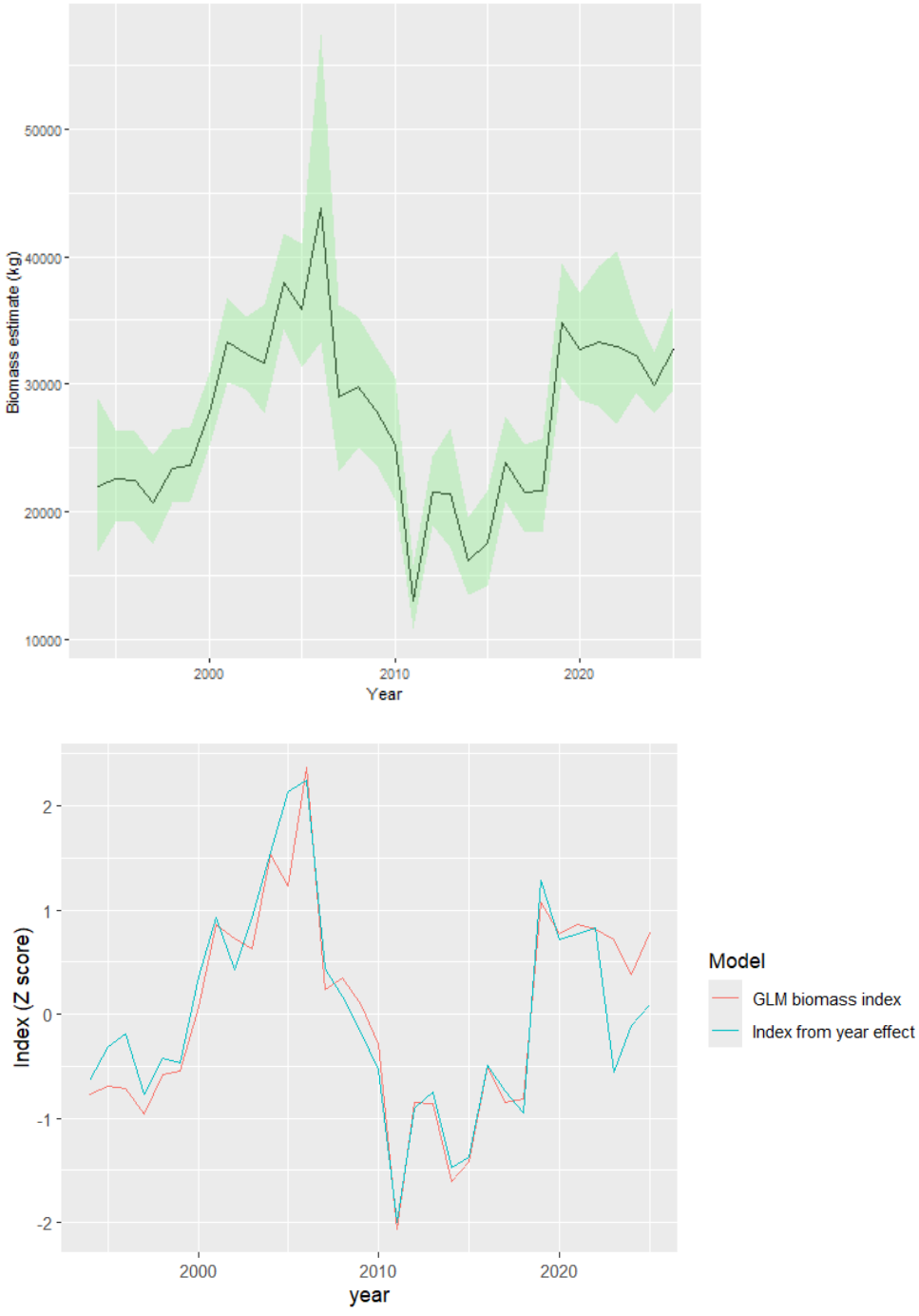


Figure 14. Abundance index estimated using the spatiotemporal GLMM (top) and comparison with the index derived from the year effect (bottom). The green band indicates 95% intervals.

The south-area abundance index showed a similar trend to the full-area index, but at a lower level and without the recent decline observed in the full-area index. The east-area index showed the same trend as the full-area index but at a much lower level (Figure 15).

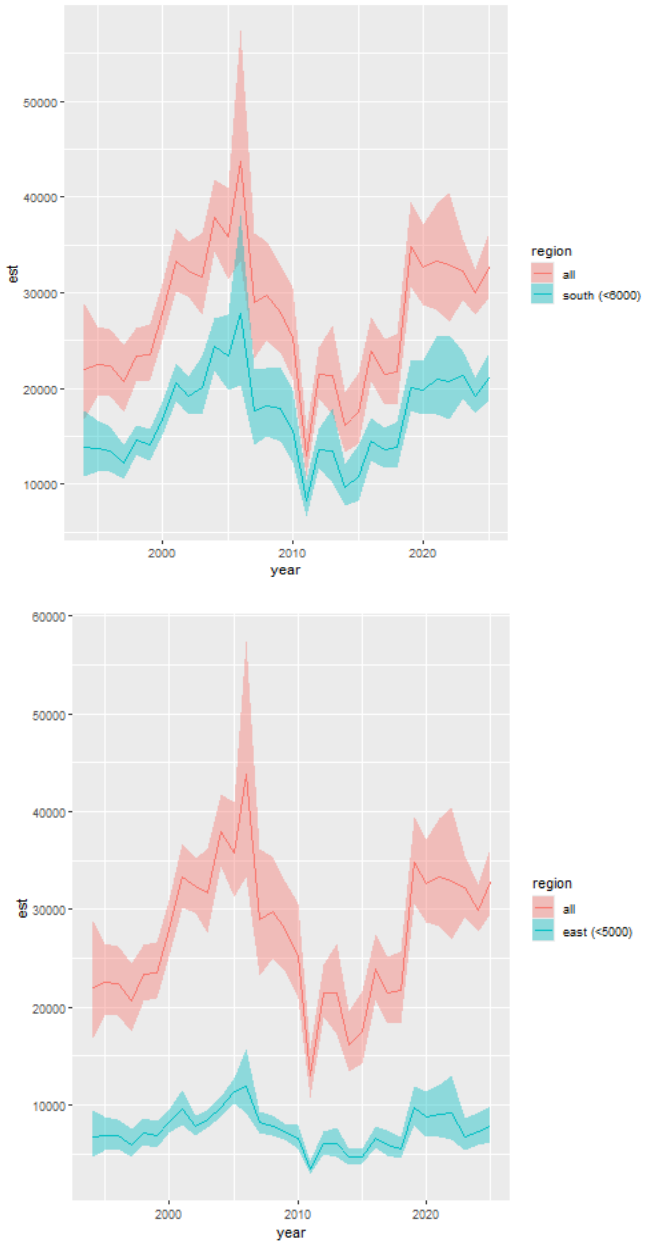


Figure 15. Abundance index for the full vs south area (top) and full vs east area (bottom). Indices based on predictions on a regular grid

Predictions from the GLMM using a regular mesh and a reference vessel (1458 m^3 hold capacity) reproduced the spatial distribution changes of the resource (Figure 16).

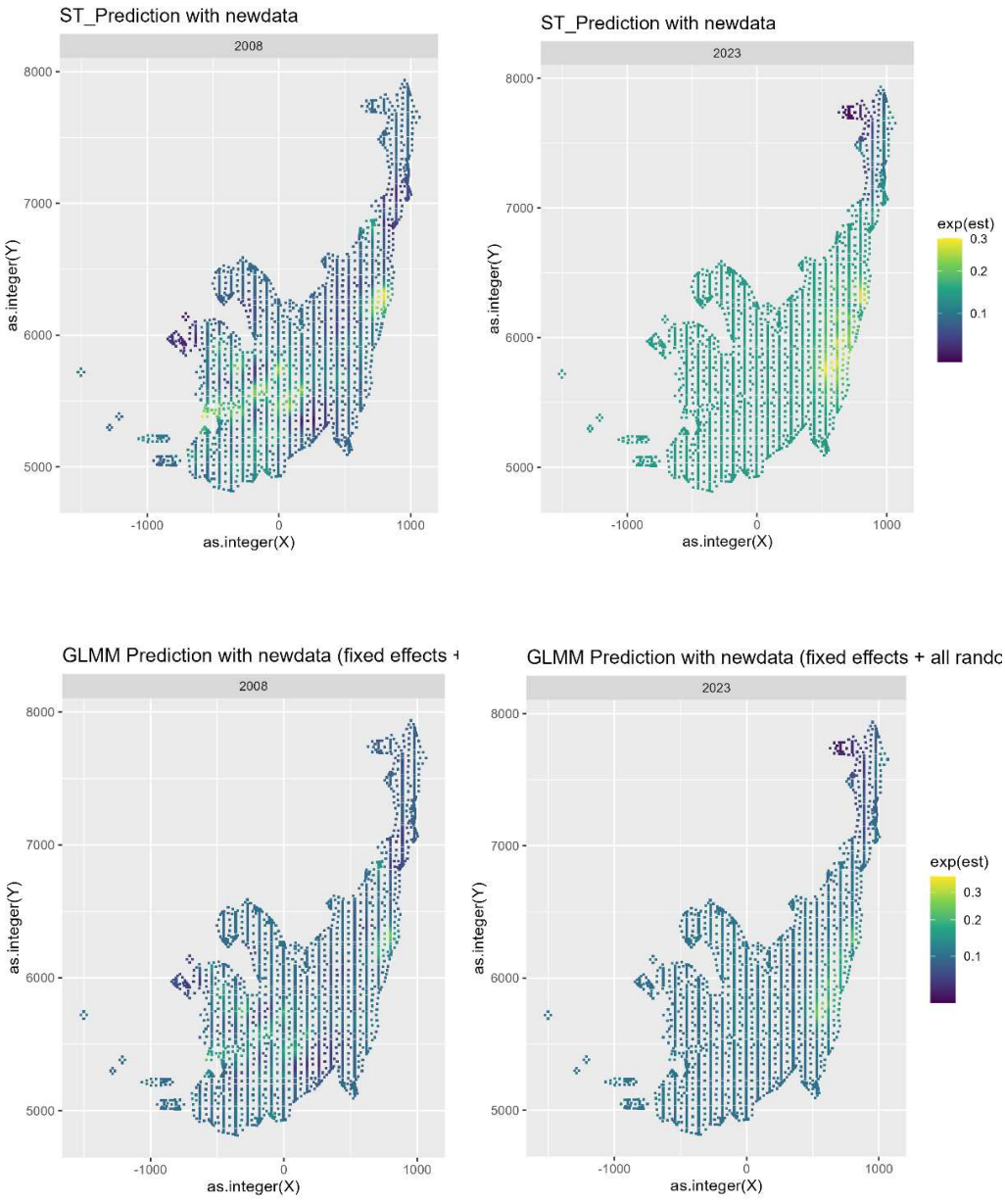


Figure 16. Examples of predictions on a regular mesh (newdata): year 2008 with a more offshore concentration (left) and year 2023 with a more coastal concentration (right).

Indices predicted by the spatiotemporal model and by the GLMM with spatiotemporal random effects using the regular mesh are shown in Figure 17.

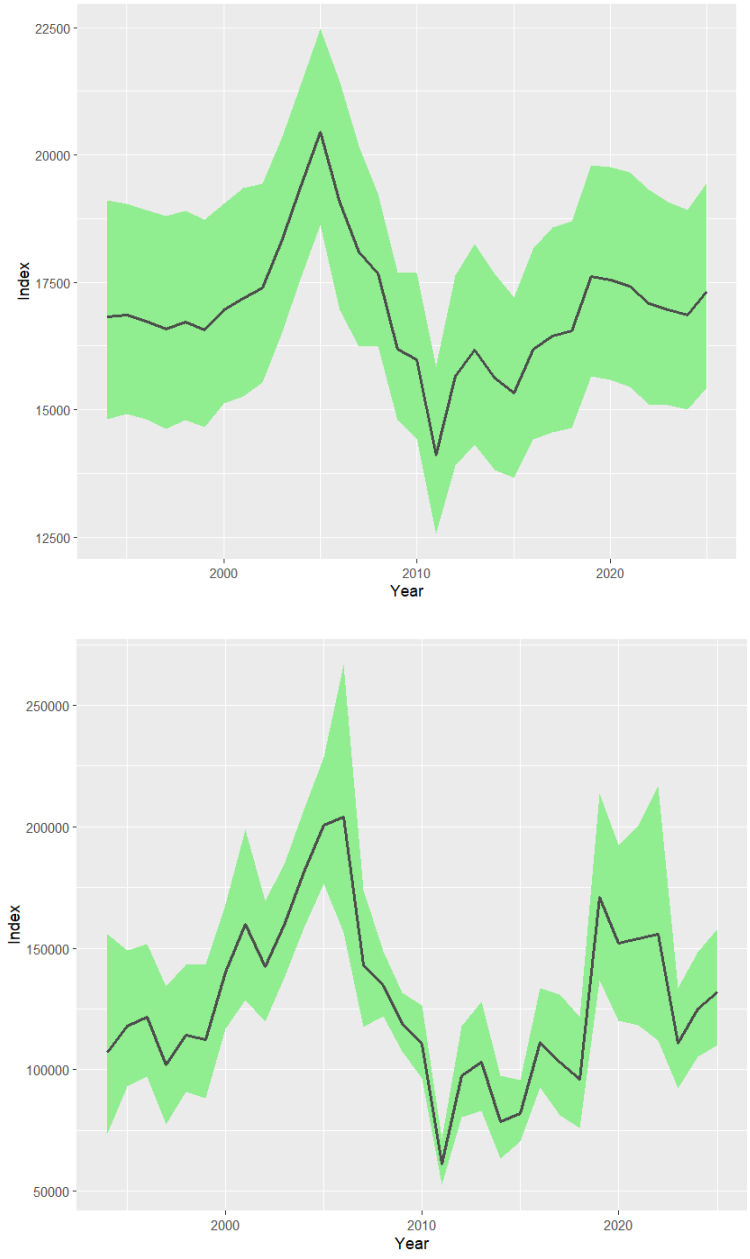


Figure 17. Index from the spatiotemporal model (top) and GLMM (bottom) using a regular mesh and a reference vessel (1458 cm^3 hold capacity).

Discussion

The abundance indices estimated by the spatiotemporal model and the spatiotemporal GLMM were not significantly different between them (Figure 18). These indices were also similar to the index estimated by Vásquez and Sepúlveda (2025) using INLA (Figure 19).



Figure 18. Abundance index estimated by the spatiotemporal GLMM (CPUE model) and the spatiotemporal model. Bands indicate 95% confidence intervals.

Compared with the traditional index used in the stock assessment model (GLM using trip-level data; Payá, 2025a), the spatiotemporal-model indices showed similar overall trends but produced lower values in the last five years (Figure 19). The index estimated by Vásquez and Sepúlveda (2025) was the closest to the traditional index during 2007–2019. This may reflect differences in how hold capacity was modelled, inclusion of days-off-port as an offset variable, and inclusion of environmental covariates (SST and chlorophyll-a).



Figure 19. Comparison among abundance indices estimated by different models in this project and those estimated by Vásquez and Sepúlveda (2025). For comparability, indices are shown for 2000–2025; years prior to 2000 are more uncertain due to small sample sizes. Values were standardised as z-scores (subtracting the mean and dividing by the standard deviation).

Using a regular mesh with a reference vessel of 1458 m^3 hold capacity produced indices with historical trends similar to those obtained using the observation-based grid, but showed a decreasing trend in the most recent years. The decrease was more pronounced for the GLMM than for the spatiotemporal model (Figure 20).

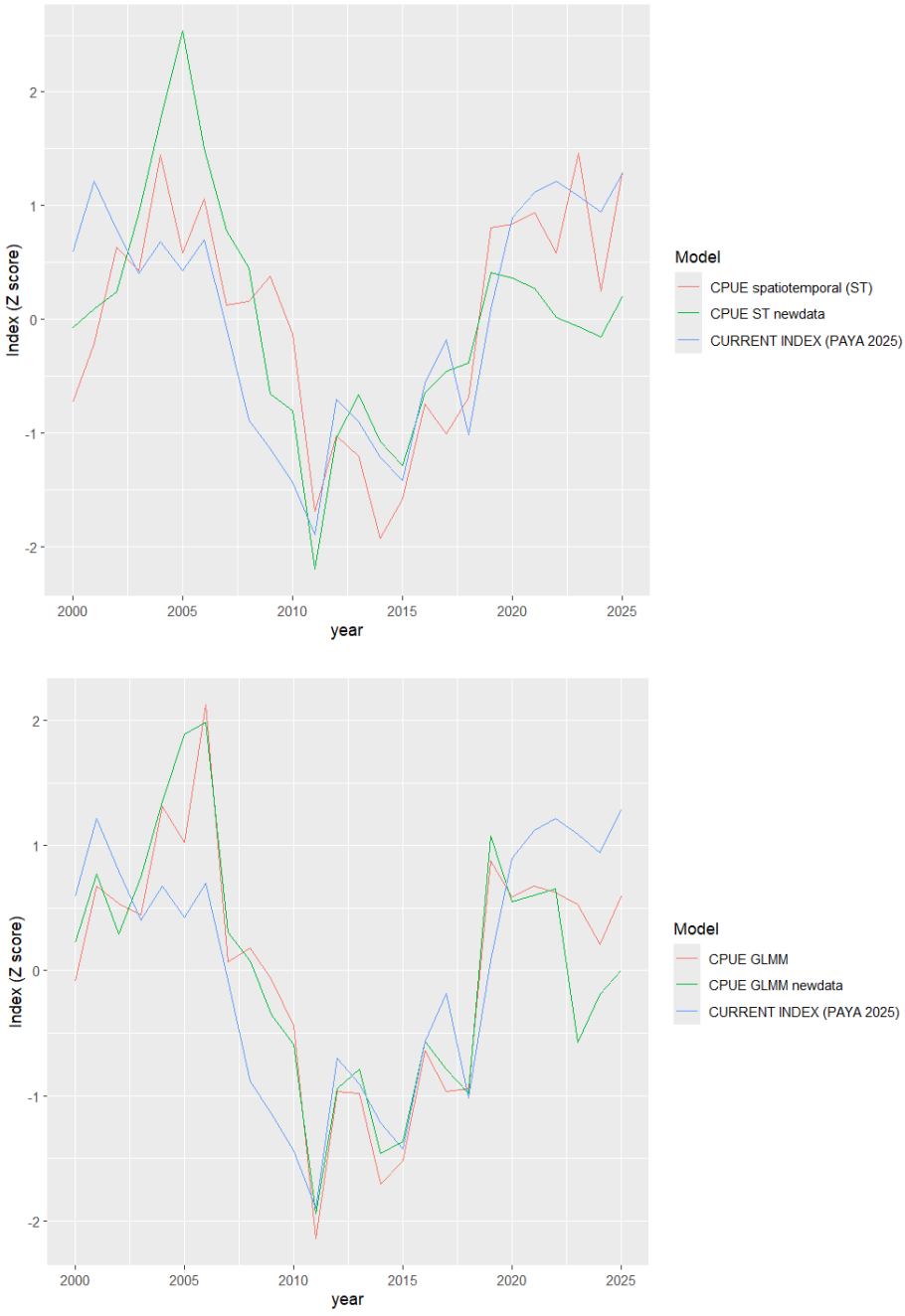


Figure 20. Estimates from spatiotemporal models (top) and GLMM (bottom) predicted using the observation-based grid and a new regular grid for a 1458 m^3 reference vessel (newdata).

The abundance index estimated as the fixed year effect from the GLMM using the original data reproduced the abundance estimates obtained using the GLMM with regular-grid predictions (Figure 21). Therefore, both approaches can be used as relative abundance indices.

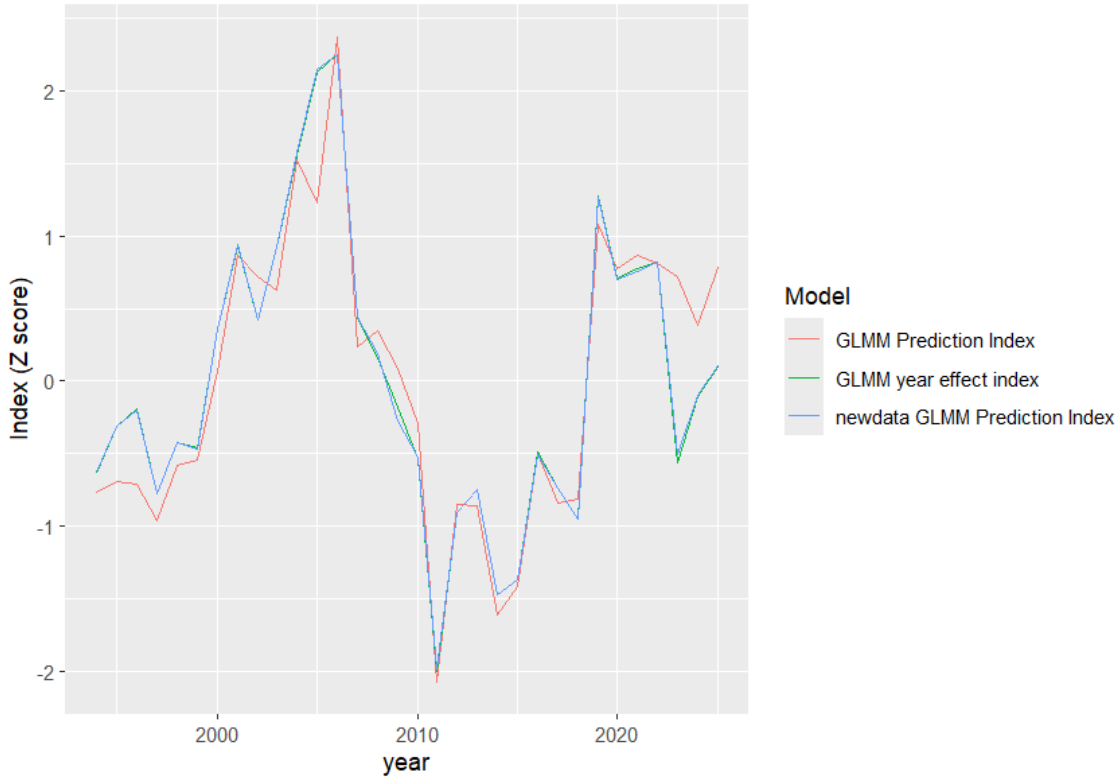


Figure 21. Indices based on spatiotemporal GLMM predictions using the original data, the fixed year effect, and predictions using new data (regular grid) for a 1458 m^3 reference vessel.

However, from year before 2000, the catch by fishing set database used in the analysis was very small compare to the whole catch in the centre-south area (Figure 22). Because of this it is recommended to use the time series from 2000.

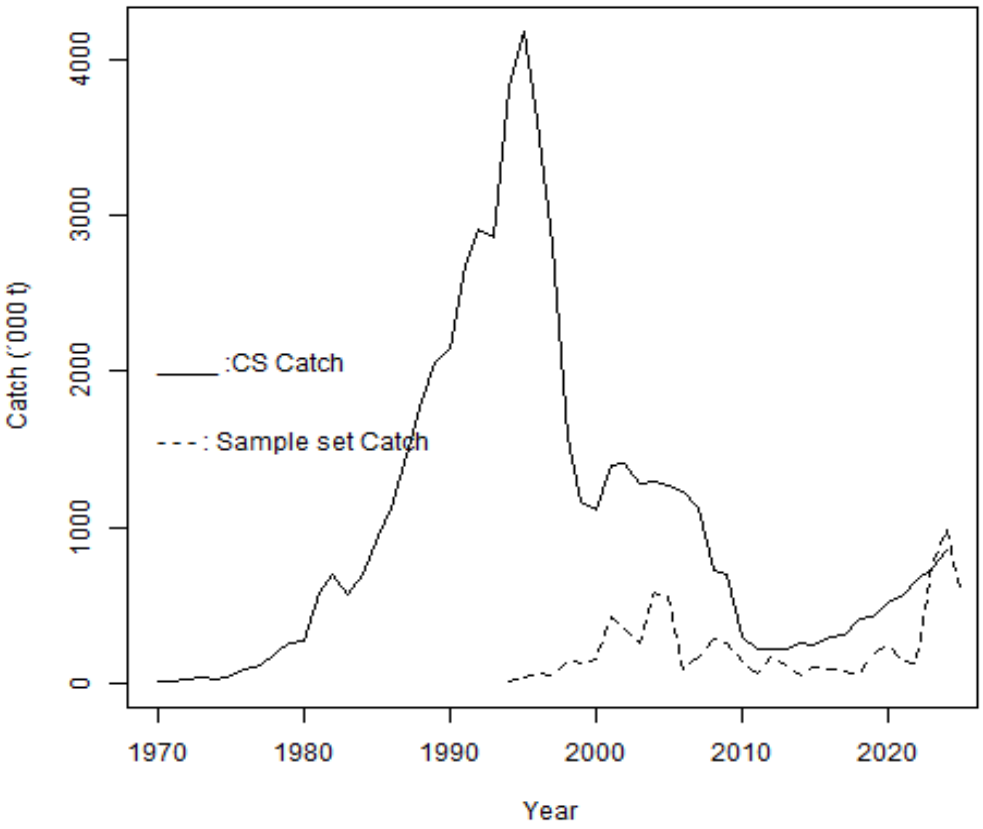


Figure 22. Whole catch in the Centre-South area (CS Catch) and in the catch by fishing set database (Sample set Catch).

Four improvements were incorporated in the current analysis compared with previous one (Payá 2023c): (1) use of SERNAPESCA electronic logbooks that covered the whole fishing fleet for 2023–2025; (2) a denser mesh with more restricted boundaries (Figure 22); (3); a significant anisotropy effect and (4) predictions on a regular grid for a reference vessel.

The main conclusion is the index estimated based on the regular mesh for reference vessel is equal to the index estimate form the year effect of the mesh with the original data. Therefore, the recommendation is to use the index based on the year effect, and taken into account the sample size, use this index starting from 2010.

References

Anderson, S.C., E.J. Ward, P.A. English, L.A.K. Barnett. 2022. sdmTMB: an R package for fast, flexible, and user-friendly generalized linear mixed effects models with spatial and spatiotemporal random fields. bioRxiv 2022.03.24.485545; doi: https://doi.org/10.1101/2022.03.24.485545.

Caballero L., J.C. Saavedra-Nievas, A. Barraza, C. Montenegro, A. Sepúlveda, C. González, S. Vargas, A. Aranis, G. Bohm y, Juan-Carlos Quiroz. (2020). CPUE Analysis of the jack mackerel purse-seine fishery of the center-south zone of Chile, June 1994 through July 2020. 15 p. SC8-JM06. SPFRMO 2020. https://www.sprfmo.int/assets/Meetings/SC/8th-SC-2020/SC8-JM06-CPUE-Analysis-CJM-purse-seine-fishery-center-south-Chile-1994-2020.pdf

Canales C., L. Caballero, y A. Aranís. 2008. Catch per Unit Effort of Chilean Jack Mackerel (*Trachurus murphyi*) of the purse seine fishery off south-central Chile (32º10' – 40º10' S) 1981-2005. Instituto de Fomento Pesquero (IFOP) - Chile. In: Chilean Jack Mackerel Workshop, SPFRMO- FAO, Santiago, mayo 2008. https://www.sprfmo.int/assets/Meetings/Meetings-before-2013/Scientific-Working-Group/Jack-Mackerel-Workshop-2008/10.CHJMWS-Catch-per-Unit-Effort-of-Chilean-Jack-Mackerel-Trachurus-murphyi-of-the.pdf.

Dunn, P. K. (2017). Tweedie: Evaluation of Tweedie exponential family models. R package version 2.3.

McCullagh, P., Nelder, John A. (1989); Generalized Linear Models, Series: Monographs on Statistics & Applied Probability, Chapman & Hall/CRC.

Payá I. (2022). High fish concentrations close to the coast in recent years could affect the Jack Mackerel CPUE abundance index in south-central Chile: proposal of a correction procedure. SC10_JM05. https://www.sprfmo.int/assets/Meetings/SC/10th-SC-2022/SC10-JM05-CPUE-abundance-index-in-south-central-Chile_update-and-proposed-correction-CL.pdf

Payá I. 2023a. Update of the Chilean Jack Mackerel CPUE abundance index based on catch by fishing trip in the south-central Chile. SC11_JM. Instituto de Fomento Pesquero.

Payá I. 2023b. Update up to June 2022 of the Chilean Jack Mackerel abundance index based on the catch per fishing set. Working document for SC11_JM. Instituto de Fomento Pesquero.

Payá I. 2023c. CJM abundance index estimated by spatiotemporal SPDE-based GLM and compare with other CPUE indices (CHL). https://www.sprfmo.int/assets/Meetings/02-SC/11th-SC-2023/Jack-Mackerel/SC11-JM12-CHL-CJM-abundance-index-estimated-by-spatiotemporal-SPDE-based-GLM-and-compare-with-other-CPUE-indices.pdf

Payá I. 2025. Jack Mackerel CPUE index and acoustic biomass in the south-central Chile up to 2025. https://www.sprfmo.int/assets/Meetings/02-SC/13th-SC-2025/Jack-

Mackerel/SC13-JM04-Jack-Mackerel-CPUE-index-and-acoustic-biomass-in-the-south-central-Chile-up-to-2025-.pdf

Acknowledgments

I thank Aquiles Sepulveda, INPESCA director, for providing the database of catch by fishing set for the period 1994-2022, recorded by the INPESCA. I am also thankful to Marlene Ramirez and Erik Gaete, IFOP scientists, for providing the IFOP database and combining it with INPESCA database.